Comparative analysis of the corneal birefringence pattern in healthy children and adults

Running head: Birefringent pattern changes in children & adults

Marcelina Sobczak[1], Magdalena Asejczyk[1], Kamil Kalinowski[1], Barbara Pierścionek[2,3]

[1] Wroclaw University of Science and Technology, Department of Optics and Photonics, Wrocław, Poland

[2] School of Life Sciences and Education, Staffordshire University, College Road, Stoke-on-Trent, ST4 2DF UK

[3] Faculty of Health, Education, Medicine and Social Care, Anglia Ruskin University, Chelmsford Campus, Bishop Hall Lane, Chelmsford CM1 QSQ UK

Corresponding author: Marcelina Sobczak, marcelina.sobczak@pwr.edu.pl

Key words: birefringence, cornea, isochromatics, isochromes, corneal structure

DISCLOSURE

The authors report no conflicts of interest and have no proprietary interest in any of the materials mentioned in this article.

ACKNOWLEDGEMENTS

This research received no specific grant from any funding agency in the public, commercial, or not-for-profit sectors.

ABSTRACT

Purpose

To undertake a comparative analysis of the corneal shape, thickness and isochromatics in the eyes of children and adults in order to determine the extent of similarities and differences between the cohorts.

Methods

The study involved 24 children (aged 8 years) and 37 young adults (aged between 22-24 years) of Caucasian origin and with no apparent or known health or ocular conditions. Measurements were made of corneal radius of curvature, corneal thickness both central (CCT) and paracentral (PCT) and intraocular pressure (IOP). Images of the isochromatics were captured using a slit lamp and a circular polarizer. The geometry of fringe I and II of the isochromatics was analyzed.

Results

Statistically significant differences were found between CCT and PCT in nasal and temporal regions in children and adult cohorts. The same trends were observed in the radii of the cornea. Statistically significant differences between side lengths and angles of isochromatic fringes were found. No differences in asymmetry of shape for fringe I between adults and children were detected; greater symmetry was seen in fringe II I in children than in adults.

Conclusions

The asymmetry in corneal shape and curvature contributes to the shape of the isochromatic fringes. This is likely to be linked to the orientation and parameters of the collagen fibers as well as to the muscles forces and be relevant for surgical procedures such as corneal transplantation.

INTRODUCTION

The optical elements of the eye: the cornea and the lens alter with age. These changes are more subtle in the cornea and, unlike the lens in which transparency decreases with age, corneal transparency is not altered.[1] The corneal changes with age pertain to shape. The cornea is flattest nasally and steepest in the temporal zone.[2] The stroma which makes up around 95% of the cornea consists of around 300 layers of collagen fibers in the center increasing to around 500 layers in the limbal region.[3,4] A number of models of fibril orientation have been proposed.[5-10] Fibril size and spacing change from the prepupillary area to the periphery of the cornea.[5] In the central cornea fibrils are closely packed and thinner than fibrils in the limbal area. The size of the collagen fibrils also alters with the depth of the stroma.[11] X-ray scattering techniques have been widely used to quantify fibril arrangement (density and orientation) in corneal stroma.[10,12,13] The results indicate that in the healthy cornea, the fibrils in the central zone have two preferred orientations – the temporal-nasal (T-N) and superior-inferior (S-I) directions–with two-thirds of the fibrils commonly aligned within the 45˚ sectors surrounding these orientations. The fibril preferential orientation then changes to circumferential at the limbus with a transition zone in the paracentral area. The depth-dependent arrangement was also observed, being more orthogonal in the posterior stroma than in the anterior lamellae.[14,15]

These changes in thickness, coupled with differences between refractive index of collagen fibrils and that of the ground substance contribute to anisotropy in the corneal structure.[16] The birefringence that is manifested is a combination of form and intrinsic birefringence with the order parameter changing from zero in the center of the cornea to a non-zero value in the limbus, with variable phase retardation and azimuth angle orientation.[17-19] Isochromatics are manifestations of a birefringent structure and the fringes represent bands of constant optical phase retardance. They are seen when the cornea is viewed in a polariscope and appear quasi-rectangular, because of the orientation of collagen lamellas.[9]

The radius of the cornea changes rapidly during the first 24 months of life.[20-22] Further increases in the corneal radius with growth and age are significantly lower.[23-25] Corneal thickness also changes with age. Ehlers et al. 1976 reported that in newborns, the central corneal thickness (CCT) is around 0.541±0.006 mm and with age the average CCT decreases up to around 0.492 mm.[21,23,26-28] Lee et al.[29] showed that the corneal thickness is greater for boys than girls in the age group between 4-9 years, reversing during adolescence when corneal thickness appears to be greater in females than in males and reversing again by adulthood.

Components of the stroma are largely collagen I, small amounts of collagen V, collagen VI, VII, VIII, XI, and a high proportion of proteoglycan and keratocytes.[16,30,31] With increasing age,

the collagen intramolecular and the interfibrillar spacing increase and the most likely cause of this is the increase in protein glycation.[32-34] In addition, the cell density is reduced and cell shape is changed.[27,34-40] Similar changes have been seen in the human, monkey, rat, cat, dog and rabbit.[41-46] The average size of cells increases with age;[27,28] there is a concomitant increase in fibril diameter[34] and a decrease in hydration stability. These alterations in structure have an effect on corneal shape with a steeping in curvature and a shift in astigmatism from with the rule to against the rule with age.[47-49]

Corneal birefringence has been studied extensively in adults[50-53] and various methods have been proposed.[51-54] Only a few studies have evaluated the age-related differences in corneal birefringence.[51,55,56] There is a paucity of studies on corneal birefringence in children. This study presents a comparative analysis of isochromatic fringes in eyes of children and young adults.

METHODS

The study participants were 24 children (15 female and 9 male) aged 8 years, recruited during vision screening tests for primary school children and 37 healthy Caucasian adults, with an age range of 22-24 years, (23 female and 14 male) recruited from the student body at the Wroclaw University of Science and Technology. All participants had a low refractive error range (± 2D (sphere); ± 0.5D (cylinder)), and had the same refractive status in both eyes (within ±0.25D) One eye from each participant was included in the study. Participants were carefully instructed, prior to each measurement, what would be required of them and the correct gaze position to adopt. None of the measurements required any contact with the eye. The project was approved by the Ethics Committee of the Faculty of Ophthalmology at the Medical Academy in Wrocław (KB 329/2014) and adhered to the Tenets of the Declaration of Helsinki. Informed consent was obtained from adult participants and informed parental consent and assent of the child were obtained from parents and children, respectively, before measurements were taken. The criteria for exclusion from the study were: any systemic disease, intraocular surgery less than six months before the study start date, refractive surgery, conjunctival or intraocular inflammation, corneal abnormalities such as oedema or scars, and contact lens wear.

Visual acuity was measured at distance and near with and without correction (Best Corrected Visual Acuity (BCVA). Radius of corneal anterior curvature was measured using a topographer E300, Medmont Pty Ltd (Melbourne, Australia). A non-contact tonometer (Corvis ST), with a Scheimpflug camera (OCULUS Optikgeräte GmbH; Wetzlar, Germany), were used to obtain intraocular pressure (IOP), central corneal thickness (CCT) and paracentral corneal thickness (PCT): nasal (PCT_N) and temporal (PCT_T). Each measurement was repeated three times.

Isochromatics were imaged with a circular polarizer fitted to a slit lamp (Digital slit lamp RS-1000 series, Righton, Japan) as shown in Figure 1A. The circular polarizer (Hoya CIR-PL) was placed just in front of the eye of each participant and acted to polarize light coming into the eye and as an analyzer for light reflected from the eye. All measurements were made between 9 am and 11 am.

Images were analyzed using customized software in MATLAB (MathWorks, Natick, MA, USA) for image processing and transformation. The analysis method was automated and confirmed manually. The preprocessing step consisted of extracting the color channel images from the raw image (see Figure 1A) and analyzing for each of the RGB color channel images separately (see Figure 1B). In each RGB channels the location of the isochromatics is different because of the phenomenon of birefringence dispersion. The iris and pupil borders and the coordinates of the pupil center were identified and the image of the iris within the border (as seen in Figure 1C) was used for further analysis. Images were transformed to cylindrical coordinates (see Figure 1D) in order to detect for the isochromatic fringe borders in peripheral area of the cornea (see Figure 1E). This enabled a definition of the inflection points (see Figure 1E - red and blue dots) which provided an estimation of angles between the sides of the quadrilateral associated with the isochromatic fringe (α_T – angle between sides of the temporal corneal side, α_U – angle between sides of the superior corneal side, α_N – angle between sides of the nasal corneal side, α_D – angle between sides of the inferior corneal side) and the lengths of the sides (B_1, B_2, B_3 and B_4) (Figure 2). This was done for the first and second fringe for all color channels (Figure 1F). Given that all color channels produced the same fringe shape and that the contrast of the red color channel was the highest; this was used as the representative result. The first and the second fringes of the isochromatics represents the changes in phase retardation values.

Reproducibility of the isochromatic fringes was tested in three children and three adults. Images of the fringes were taken twice more after the initial image capture: after one-week (to enable assessment of longer repeatability). Images were compared by superimposition and processing by Matlab® to determine any changes in shape of the isochromatic fringes. Image were consistently reproducible in all obtained cases with a maximum of 2% error.

Statistical analysis was conducted using STATISTICA ver. 13.3 (StatSoft, Inc., USA). All data were first tested for normality; as normality was rejected in the majority of cases (p<0.05) given skewness in the data distribution non-parametric statistical tests were used. Brown-Forsythe and Levene's were used to test the hypothesis of equal variance. The Wilcoxon rank-sum test was used to compare the median difference of the angles (α_T, α_U, α_N, α_D) and lengths of the sides (B_1, B_2, B_3 and B_4) of the isochromatics, as well as differences of corneal radii and corneal thicknesses, and differences between adult and children's eyes. Statistical significance was taken at p-values < 0.05.

RESULTS

The mean (±SD) and range of anterior axial corneal radius of curvature and in horizontal (nasal (R_N) and temporal (R_N)) and vertical (up (R_U) and down (R_D)) sections as 3.5 mm from pupil center, central corneal thickness (CCT), paracentral corneal thickness for nasal (PCT_N) and temporal (PCT_T)) side and intraocular thickness (IOP) are shown in Table 1. There are statistically significant differences (Wilcoxon test, $p<0.05$) between median CCT, PCT_T, PCT_N within groups of adults and children but the ranges are similar.

Figure 3 shows boxplots of mean, median and outliner values of corneal radii (R_A , R_T, R_N, R_U, R_D) (Figure 3A) and corneal thickness (CCT, PCT_T, PCT_N) (Figure 3B) in groups of children and adults. The lowest value of corneal radius was obtained at the corneal apex (R_A) and the highest at the nasal side of the cornea (R_N). The differences between these radii are statistically significant (Wilcoxon test, $p<0.005$) both in the child and adult cohorts (Table 2). The same trend was observed in the thickness of the cornea: the thinnest part of the cornea was in the center (CCT) and the thickest on the nasal side (PCT_N). Statistically significant differences were found between CCT, PCT and PCT in both children and adults (Table 2). The corneal radius in the upper (R_U) and lower (R_D) parts was similar (Wilcoxon test, $p>0.1$) in groups of children and adults.

Figure 4 shows examples of isochromatic fringes in corneas of adults (Figures 4A and 4B) and children (Figures 4C and D). Distortion of the isochromatics (fringe I and II) and asymmetry from the nasal side of the cornea is noticeable in all images. This asymmetry is reflected in the differences in the length of the diagonal sides (B_1, B_2, B_3 and B_4) and the values of the vertex angles (α_T, α_U, α_N, α_D) of the quadrilateral representing the isochromatic pattern (see Figure 2). The mean lengths of the sides and the angle values of the isochromatics (for red color channel as representative) in children and adults are given in Table 3. The distribution of the average values of the lengths of individual sides and angles is presented on the boxplots in Figure 5. Table 4 shows the results of the Wilcoxon test (*p*-value) for comparison of medians of sides (B_1, B_2, B_3 and B_4) and angles (α_T, α_U, α_N, α_D) of the isochromatics; the first (I) and second (II) fringes. The longest side of fringe I as well as of fringe II was obtained for B_3 (nasal side downwards) both in adult (Figure 5A) and child cohorts (Figure 5B). In fringe I, the shortest side is B_4 (temporal side downward) (Table 3). Statistically significant differences were found between lengths of all sides in adults (Table 4, column 2) and for 5 of 6 considered pairs of sides in children (Table 4, column 4).

The asymmetry of the isochromatic fringe is also reflected in the differences between the values of its vertex angles. In both groups, for fringe I the nasal angle (α_N) is the smallest of the angles (Figure 5C and D) and significantly differs from the other angles (Table 4, column 2 (adults), column 4 (children)). Similarity was found only between α_U and α_D (Wilcoxon test,

p>0.05) in both groups and between α_T vs. α_U and α_T vs. α_D for children. The differences in the results between adult and child cohorts appear for fringe II. For fringe II, the asymmetry is slightly smaller for adults and no statistically significant difference was found between sides B_1 vs B_2 and B_2 vs B_3 and between the angles α_T vs α_D, α_U vs α_D in group adults (Table 4, column 3).

Despite the statistically significant asymmetry of fringe I in the group of children, fringe II shows some symmetry; the differences between the sides lengths are not statistically significant, while the values of vertex angles showed smaller significant differences (Figures 5B and D) than in the adult group (Figures 5A and C). For fringe II in children, significant differences (p<0.05) were found between two pairs of vertex angles, namely between α_U vs. α_N and α_N vs. α_D, see Table 4.

Figure 6 shows values of distance between fringes I and II on temporal (I-II$_T$) and nasal (I-II$_N$) sides in both groups; children and adults. Comparative analysis of the distances between fringes showed a statistical significance difference (Wilcoxon test, p<0.05) between temporal side and nasal side of cornea, p=0.002 and p<0.001 for child and adult cohorts, respectively. The mean distance between fringes on the temporal side is larger than on nasal side of the cornea for both groups. However, there is no correlation (R-Spearman) between fringe distance and corneal thickness on the nasal side and temporal sides of the cornea; in the adult cohort: PCT$_T$ vs I-II$_T$, R=0.027, p=0.790 and PCT$_N$ vs. I-II$_N$, R=0.049, p=0.886, in the child cohort: PCT$_T$ vs. I-II$_T$, R=0.177, p=0.863 and PCT$_N$ vs. I-II$_N$, R=0.168, p=0.602.

DISCUSSION

The utilization of polarized light as a tool for discerning corneal structure and as a potential means of early diagnosis of corneal pathologies has been highlighted in recent years.[57-59] Isochromatics are seen in high ordered crystals and in biological tissues that are composed of layers of long fiber cells, such as the cornea and eye lens.[60] Seminal research by scientific luminaries reported measurements of intrinsic and form birefringence in molecules and cells.[61,62] Intrinsic birefringence, which arises at the molecular/cellular level, and form birefringence, caused by the layered arrangement of elongated cells and/or molecules, together determine the overall birefringence. The lamellar organization of the corneal stroma produces form birefringence and can provide information about the fibril orientation.[63] The findings show that isochromatics are not rotationally symmetrical but rather distorted and elongated towards the nasal side forming a quasi-rhomboid.

Irsch et al.[56] investigated birefringence of the central cornea scanning laser polarimetry (GDx-VCC^{TM}, Carl Zeiss Meditec, Inc.). They found no significant relationship between central

corneal birefringence and age in a cohort ranging from 3 to 70 years. These findings are in accordance with literature reports on structural change of the central cornea with age.[34,64] Although substantial changes in central corneal thickness occur in infancy and in very early childhood, the structure of the central cornea, and in particular the structure and thickness of the stroma, which give rise to corneal birefringence from the lamellar arrangement of collagen fibers, essentially reach adult values at about six months after birth,[64] with only small structural changes occurring thereafter.[34] However, Gogola et al.[65] analyzed the tortuosity of collagen in the corneae aged from 1 month to 97 years and found that these parameters show a significant monotonic decrease with age in the central and peripheral cornea and limbus.

Fukuda et al.[57] did not find significant differences in corneal thickness nor phase retardation between younger (mean age 23±1 years) and older (mean 66±8 years) subjects using Polarization Sensitive-OCT. Significant differences are seen in thickness and radii of curvature between central and peripheral regions as well as between nasal and temporal sections (Table 2) suggesting that the asymmetry is present from early years and is retained rather than that it develops with age or is influenced by the well documented change in corneal toricity with age, namely that of with the rule to against the rule astigmatism.[48,49] The asymmetry in corneal shape and curvature contributes to the shape of the isochromatics which present as a skewed four-sided fringe pattern with the nasal angle smaller than the temporal angle. This is seen in both adult and child cohorts although the latter appear to show slightly more symmetry (Figure 4) This may arise because of subtle variations in corneal thickness and radii of curvature between nasal and temporal sections that may be greater in adults than in children. However, these are not significantly different, as seen in Table 1 (Figure 3). Radii of curvature in the central and peripheral sections do not vary significantly between child and adult cohorts; central and peripheral thickness, however, does (Table 1). No differences were found between superior and inferior corneal radii (Table 2, Figure 3).

In both child and adult cohorts both the quadrant lengths of the isochromatics and their angles vary from one other (Table 3, Figure 5). In both age groups these differences are statistically significant for fringe I, indicative of the asymmetry seen in both cohorts (Table 4).

For fringe II the differences between side lengths and angles are statistically significant in the adult group, while in children, this fringe shows greater symmetry. This finding may be related to the statistically significant changes of the waviness and the tortuosity of the collagen fibers in the peripheral cornea with age, as described by Gogola et al.[65]

Fukuda et al.[58] reported that the phase retardation values measured in the central 6mm diameter corneal area is higher than in the central 3 mm diameter area and that this applies for normal and keratoconic eyes. These findings indicate that the corneal curvature changes with progression from the apex and this phenomenon is reflected in the shape of the

isochromatics and in the distances between the isochromatic fringes. Scattering methods have revealed a preferential orientation of collagen fibrils in the central cornea in the superior–inferior and nasal–temporal directions. [9,10,17]

The results of our study show that inter-fringe distances differ with statistical significance between temporal and nasal sides in both age groups (Figure 6). An explanation of this asymmetry may be because of the thickness differences between the nasal and temporal cornea. Given that isochromatic fringes are lines of constant optical phase retardation, another cause for the lack of symmetry could be the asymmetric distribution of the extraocular muscle forces. The vertices of the isochromatic fringes map onto the approximate positions of attachment of the four lateral recti muscles. While in the vertical direction these muscles show a certain symmetry, both in the geometric and initial tension force, there is a significant difference between the medial rectus and lateral recti muscles.[66] Gao et al.[66] estimated the initial tension forces of the extraocular muscles to be 48.87-14.2mN for the lateral rectus, 89.27-31.6mN for the medial rectus, 50.7-17.6mN for the superior rectus, 46.27 13.4mN for the inferior rectus. The distance from the corneal limbus of the medial rectus attachment is 5.5mm whereas it is 9mm for the lateral rectus. This can directly influence the force applied to the cornea along the horizontal axis and such asymmetry could be reflected in the shape of the isochromatics.[53] Boote et al.[10] have been suggested that different orientation of corneal lamellas exist to take up the stress exerted on the cornea by the ocular motor muscles, thereby helping to preserve corneal shape. They demonstrated a higher density of collagen fibrils in the sclera at the four cardinal points outside the cornea that are directed toward the extraocular muscles, they concluded that this collagen fibrils may have a mechanical function related to eye movement. It has been suggested from measurements of photo-stress analysis tomography, that the orientation of collagen fibrils represents a favorable stress distribution for eye movements.[67]

If indeed the shape of the isochromatics is determined by the work of the extraocular muscles and this is cumulative effect over years, it could be expected that these figures would be less distorted in the corneas of children. Yet, this was not the case. The asymmetries in corneal shape may have the greater effect and/or the impact of the extraocular muscles is already evident in childhood.

It is worth noting that previous studies that have measured birefringence of the cornea was concerned with measurement in the corneal regions which are pertinent to vision[50] and using polarized light as a potential means of diagnosis.[51, 56-59] Previous research took into account the azimuth when measuring polarization properties of the central cornea[50,56] and tried to determine the corneal polarization axis and magnitude in healthy and glaucomatous eyes in order to adequately correct for corneal birefringence in studies of birefringence in the retinal

fiber layer.[51] For proper characterization of birefringence of the cornea and use of this characteristic in disease diagnosis requires sophisticated methods such Polarization Sensitive Optical Coherence Tomography (PS-OCT) which can image corneal structure at the microscopic level.[57-59] This study is not concerned with measuring corneal birefringence in the central regions but with the isochromatics in the peripheral cornea.

The implications of these findings may be on surgical procedures, both current and developing methods including future advances in cultured corneal tissue for transplantation. Any transplantation, whether full thickness such as penetrating keratoplasty or partial such as deep anterior lamellar keratoplasty, compromises corneal mechanical properties and disrupts structure. This could have an effect on optical quality and ultimately on success of the implant. Transmission of extraocular muscle forces on the cornea will vary depending on fibril orientation and this would manifest in the shape and numbers of isochromatic fringes. Transplantation success could be achieved by optimizing position of the surgical incision and orientation of the transplanted tissue with respect to the cornea. Isochromatics may prove pivotal to this success. Future transplantation methods should take into account the importance of preserving the integrity of the lamellar structure of the cornea and the value of the isochromatic fringes.

REFERENCES

1. van den Berg TJ & Tan KE. Light transmittance of the human cornea from 320 to 700 nm for different ages. Vision Res 1994; 34(11): 1453–1456.
2. Sinjab MM. Corneal Optics and Geometry. Corneal Tomography in Clinical Practice (Pentacam System): Basics and Clinical Interpretation. 3rd ed. Jaypee Brothers Medical Publishers: New Dehli, 2019; pp. 3-7.
3. Misson GP. The theory and implications of the biaxial model of corneal birefringence. Ophthalmic Physiolog 2010; 30(6): 834-846.
4. Radner W, Zehetmayer M, Aufreiter R & Mallinger R. Interlacing and cross-angle distribution of collagen lamellae in the human cornea. Cornea 1998; 17(5): 537–543.
5. Boote C, Kamma-Lorger CS, Hayes S, et al. Quantification of Collagen Organization in the Peripheral Human Cornea at Micron-Scale Resolution. Biophys J 2011; 101(1): 33-42.
6. Meek KM & Boote C. The organization of collagen in the corneal stroma. Exp Eye Res 2004; 78(3): 503–512.
7. Pinsky PM, van der Heide D & Chernyak D. Computational modeling of mechanical anisotropy in the cornea and sclera. J Cataract Refr Surg 2005; 31(1): 136-145.
8. Misson GP. Circular polarization biomicroscopy: a method for determining human corneal stromal lamellar organization in vivo. Ophthal Physl Opt 2007; 27(3): 256-264.
9. Boote C, Dennis S, Huang Y, Quantock AJ & Meek KM. Lamellar orientation in human cornea in relation to mechanical properties. J Struct Biol 2005; 149(1): 1–6.
10. Boote C, Hayes S, Abahussin M & Meek KM. Mapping collagen organization in the human cornea: left and right eyes are structurally distinct. Invest Ophthalmol Vis Sci 2006; 47(3): 901-908.
11. Blackburn BJ, Jenkins MW, Rollins AM & Dupps WJ. A Review of Structural and Biomechanical Changes in the Cornea in Aging, Disease, and Photochemical Crosslinking. Front Bioeng Biotechnol 2019; 7: 66.
12. Aghamohammadzadeh H, Newton RH & Meek KM. X-Ray Scattering Used to Map the Preferred Collagen Orientation in the Human Cornea and Limbus. Structure 2004; 12(2): 249–256.
13. Meek KM, Blamires T, Elliott GF, Gyi TJ & Nave C. The organisation of collagen fibrils in the human corneal stroma: a synchrotron X-ray diffraction study. Curr Eye Res 1987; 6(7): 841–846.
14. Benoit A, Latour G, Marie-Claire S-K & Allain J-M. Simultaneous microstructural and mechanical characterization of human corneas at increasing pressure. J Mech Behav Biomed Mater 2016; 60: 93–105.
15. Abahussin M, Hayes S, Cartwright NEK, et al. 3D collagen orientation study of the human cornea using X-ray diffraction and femtosecond laser technology. Investig Ophthalmol Vis Sci 2009; 50(11): 5159–5164.
16. Meek KM & Knupp C. Corneal structure and transparency. Prog Retin Eye Res 2015; 49: 1-16.
17. Daxer A & Fratzl P. Collagen fibril orientation in the human corneal stroma and its implication in keratoconus. Invest Ophthalmol Visual Sci 1997; 38: 121–129.
18. Pandolfi A & Manganiello F. A model for the human cornea: constitutive formulation and numerical analysis. Biomech Model Mechanobiol 2006; 5: 237–246.
19. Knighton RW, Huang XR & Cavuoto LA. Corneal birefringence mapped by scanning laser polarimetry. Opt Express 2008; 16: 13738–13751.
20. Gordon RA & Donzis PB. Refractive Development of the Human Eye. Arch Ophthalmol 1985; 103: 785-789.

21. Ehlers N, Sorensen T, Bramsen T & Poulsen EH. Central corneal thickness in newborns and children. Acta Ophthalmol 1976; 54(3): 285-290.
22. Flitcroft DI, Knight-Nanan D, Bowell R, Lanigan B & O'Keefe M. Intraocular lenses in children: changes in axial length, corneal curvature, and refraction. Br J Ophthalmol 1999; 83: 265-269.
23. Doughty MJ, Laiquzzaman M, Müller A, Oblak E & Button NF. Central corneal thickness in European (white) individuals, especially children and the elderly, and assessment of its possible importance in clinical measures of intra-ocular pressure. Ophthal Physiol Opt 2002; 22: 491-504.
24. Tomlinson A. A clinical study of the central and peripheral thickness and curvature of the human cornea. Acta Ophthalmol 1972; 50: 73-82.
25. Hashemi H, Asgari S, Emamian MH, Mehravaran S & Fotouhi A. Age-Related Changes in Corneal Curvature and Shape: The Shahroud Eye Cohort Study. Cornea 2015; 34(11): 1456-1458.
26. Alsbirk PH. Corneal thickness: I. Age Variation, Sex Difference and Oculometric Correlations. Acta Ophthalmol 1978; 56(1): 95-104.
27. Galgauskas S, Norvydaite D, Krasauskaite D, Stech S & Asoklis RS. Age-related changes in corneal thickness and endothelial characteristics. Clin Interv Aging 2013; 8: 1445-1450.
28. Islaml QU, Saeed MK & Mehboob MA. Age related changes in corneal morphological characteristics of healthy Pakistani eyes. Saudi J Ophthalmol 2017; 31(2): 86-90.
29. Lee D-H, Kim D-H & Park S-H. Age and Sex Related Changes in Corneal Thickness and Anterior Corneal Curvature in Korean Young Population with Orbscan II Topography System. J Opt Soc Korea 2011; 15(1): 68-73.
30. Newsome DA, Foidart JM, Hassell JR, et al. Detection of specific collagen types in normal and keratoconus corneas. Invest Ophthalmol Vis Sci 1981; 20: 738–750.
31. Espana EM &Birk DE. Composition, structure and function of the corneal stroma. Exp Eye Res 2020; 198: 108137.
32. Malik NS, Moss SJ, Ahmed N, et al. Ageing of the human corneal stroma: structural and biochemical changes. Biochim Biophys Acta 1992; 1138: 222–228.
33. Malik NS & Meek KM. Vitamins and analgesics in the prevention of collagen ageing. Age Ageing 1996; 25: 279–284.
34. Daxer A, Misof K, Grabner B, Ettl A & Fratzl P. Collagen fibrils in the human corneal stroma: structure and aging. Invest Ophthalmol Vis Sci 1998; 39: 644–648.
35. Berlau J, Becker H-H, Stave J, Oriwol C & Guthoff RF. Depth and age-dependent distribution of keratocytes in healthy human corneas: a study using scanning-slit confocal microscopy in vivo. J Cataract Refract Surg 2002; 28: 611–616.
36. Niederer RL, Perumal D, Sherwin T & McGhee CNJ. Age-related differences in the normal human cornea: a laser scanning in vivo confocal microscopy study. Br J Ophthalmol 2007; 91: 1165–1169.
37. Gipson IK. Age-related changes and diseases of the ocular surface and cornea. Invest Ophthalmol Vis Sci 2013; 54: ORSF48–ORSF53.
38. Gambato C, Longhin E, Catania AG, et al. Aging and corneal layers: an in vivo corneal confocal microscopy study. Graefe Arch Clin Exp Ophthalmol 2015; 253: 267–275.
39. Zheng T, Le Q, Hong J & Xu J. Comparison of human corneal cell density by age and corneal location: an in vivo confocal microscopy study. BMC Ophthalmol 2016; 16: 109.
40. Kanai A & Kaufman HE. Electron microscopic studies of corneal stroma: aging changes of collagen fibers. Ann Ophthalmol 1973; 5: 285–287.
41. Murphy C, Alvarado J, Juster R & Maglio M. Prenatal and postnatal cellularity of the human corneal endothelium. Invest Ophthalmol Vis Sci 1984; 25: 312–22.

42. Baroody RA, Bito LZ, Derousseau CJ & Kaufman P. Ocular development of ageing. I Corneal endothelial changes in cats and in free-ranging and caged rhesus monkeys. Exp Eye Res 1987; 45: 607–622.
43. Fitch KL, Nadakavukaren MJ & Richardson A. Age-related changes in the corneal endothelium in the rat. Exp Gerontol 1982; 17: 179–183.
44. MacCallum DK, Bahn CF, Lillie JH, Meyer RF & Martonyi CL. Evidence for corneal endothelial cell hypertrophy during postnatal growth of the cat cornea. Invest Ophthalmol Vis Sci 1983; 24: 247–50.
45. Gwin RM, Lerner I, Warren JK & Gum G. Decrease in canine corneal endothelial cell density and increase in corneal thickness as functions of age. Invest Ophthalmol Vis Sci 1982; 22(2): 267-271.
46. Oh JO. Changes with age in the cornea of normal rabbits. Acta Ophthalmol 1963; 41: 568–573.
47. Hayashi K, Masumoto M, Fujino S & Hayashi F. Changes in corneal astigmatism with age. Nippon Ganka Gakkai Zasshi 1993; 97: 1193–1196.
48. Hayashi K, Hayashi H & Hayashi F. Topographic analysis of the changes in corneal shape due to ageing. Cornea 1995; 14: 527–532.
49. Shao X, Zhou K-J, Pan A-P, et al. Age-Related Changes in Corneal Astigmatism. J Refracr Surg 2017; 33(10): 696-703.
50. Knighton RW & Huang XR. Linear birefringence of the central human cornea. Invest Ophthalmol Vis Sci 2002; 43(1): 82–86.
51. Weinreb RN, Bowd C & Greenfield DS. Measurement of the magnitude and axis of corneal polarization with scanning laser polarimetry. Arch Ophthalmol 2002; 120(7): 901–906.
52. Mastropasqua R, Nubile M, Salgari N, et al. Interference figures of polarimetric interferometry analysis of the human corneal stroma. PLoS ONE 2017; 12(6): e0178397.
53. Beer F, Wartak A, Haindl R, et al. Conical scan pattern for enhanced visualization of the human cornea using polarization sensitive OCT. Biomed Opt Express 2017; 8(6): 2906-2923.
54. Zhou Q & Weinreb RN. Individualized compensation of anterior segment birefringence during scanning laser polarimetry. Invest Ophthalmol Vis Sci 2002; 43(7): 2221–2228.
55. Mai TA & Lemij HG. Longitudinal measurement variability of corneal birefringence and retinal nerve fiber layer thickness in scanning laser polarimetry with variable corneal compensation. Arch Ophthalmol 2008; 126(10): 1359–1364.
56. Irsch K & Shah AA. Birefringence of the central cornea in children assessed with scanning laser polarimetry. J Biomed Opt 2012; 17(8): 086001.
57. Fukuda S, Kishino G, Hoshi S, et al. Repeatability of Corneal Phase Retardation Measurements by Polarization-Sensitive Optical Coherence Tomography. Invest Ophthalmol Vis Sci 2015; 56(5): 3196-3201.
58. Fukuda S, Yamanari M, Lim Y, et al. Keratoconus Diagnosis Using Anterior Segment Polarization-Sensitive Optical Coherence Tomography. Investig Ophthalmol Vis Sci 2013; 54: 1384-1391.
59. Fukuda S, Beheregaray S, Kasaragod D, et al. Noninvasive evaluation of phase retardation in blebs after glaucoma surgery using anterior segment polarization-sensitive optical coherence tomography. Invest Ophthalmol Vis Sci 2014; 55: 5200–5206.
60. Pierscionek BK & Regini JW. The gradient index lens of the eye: an opto-biological synchrony. Prog Ret Eye Res 2012; 31(4): 332-349.
61. Perutz MF. Polarization, dichroism, form birefringence, and molecular orientation in crystalline haemoglobins. Acta Cryst 1953; 6: 589-864.

62. Bragg WL & Pippard AB. The form birefringence of macromolecules. Acta Cryst 1953; 6: 865-867.
63. Götzinger E, Pircher M, Sticker M, Fercher A & Hitzenberger CK. Measurement and imaging of birefringent properties of the human cornea with phase-resolved, polarization-sensitive optical coherence tomography. J Biomed Opt 2004; 9(1): 94–102.
64. Lesueur L, Arne JL, Mignon-Conte M & Malecaze F. Structural and ultrastructural changes in the developmental process of premature infants' and children's corneas. Cornea1994; 13(4): 331–338.
65. Gogola A, Jan N-J, Brazile B, et al. Spatial Patterns and Age-Related Changes of the Collagen Crimp in the Human Cornea and Sclera. Invest Ophthalmol Vis Sci 2018; 59(7): 2987-2998.
66. Gao Z, Guo H & Chen W. Initial tension of the human extraocular muscles in the primary eye position. J Theor Biol 2014; 353: 78-83.
67. Anthony SJ. Imaging shear stress distribution and evaluating the stress concentration factor of the human eye. Sci Rep 2015; 5:8899.

TABLES AND FIGURES

Table 1. Mean (±SD) corneal radii (R_A, R_T, R_N, R_U, R_D), CCT and PCT (PCT_N, PCT_T) and IOP for adult and children cohorts. Results of comparison between adults and children (Wilcoxon test, p-value)

	Adults mean±SD	**Children** mean±SD	***p*-value**
R_A [mm±SD]	7.9±0.3 (7.3÷8.8)	8.0±0.4 (7.6÷8.6)	0.259
R_T [mm±SD]	8.2±0.3 (7.4÷9.0)	8.4±0.4 (7.9÷9.0)	0.373
R_N [mm±SD]	8.5±0.4 (7.6÷9.6)	8.6±0.3 (8.1÷9.1)	0.373
R_U [mm±SD]	8.0±0.3 (7.3÷8.7)	8.3±0.4 (7.7÷8.9)	0.082
R_D [mm±SD]	8.0±0.4 (7.4÷8.9)	8.3±0.4 (7.7÷8.9)	0.072
CCT [μm±SD]	545±34 (492÷640)	572±28 (533÷624)	0.008*
PCT_T [μm±SD]	602±39 (542÷681)	634±28 (583÷686)	0.011*
PCT_N [μm±SD]	665±34 (607÷729)	699±36 (649÷764)	0.011*
IOP [mmHg±SD]	16.3±2.4 (12.7÷20.4)	14.9±2.3 (11.3÷17.9)	0.166

* denotes statistical significance

Table 2. Wilcoxon test (*p*-value) for comparison of median corneal radii and corneal thickness in the vertical section

	Adults *p*-value	**Children** *p*-value
R_A vs. R_T	<0.001*	0.002*
R_A vs. R_N	<0.001*	0.002*
R_N vs. R_T	<0.001*	0.029*
R_U vs. R_D	0.516	0.414
CCT vs. PCT_T	<0.001*	0.002*
CCT vs. PCT_N	<0.001*	0.002*
PCT_N vs. PCT_T	<0.001*	0.002*

* denotes statistical significance

Table 3. Mean (±SD) of the lengths of the sides (B_1, B_2, B_3 and B_4) angles (α_T –temporal part, α_U – upper part, α_N –nasal part, α_D – down part of cornea) of isochromatics of first (I) and second (II) fringes using the red color channels

	Adults		Children	
	fringe I	**fringe II**	**fringe I**	**fringe II**
B_1 [px±SD]	1282 ± 125	1436±162	1280±80	1445±78
B_2 [px±SD]	1232 ± 115	1455±197	1209±78	1418±138
B_3 [px±SD]	1413 ± 97	1559±206	1357±111	1451±178
B_4 [px±SD]	1164 ± 134	1324±199	1155±123	1436±200
α_T [°±SD]	94.7 ± 6.3	95.1±10.1	90.8±5.7	88.4±7.4
α_U [°±SD]	91.6 ± 5.3	90.6±5.5	93.0±4.5	91.3±4.7
α_N [°±SD]	85.5 ± 5.8	84.3±7.8	84.8±4.2	88.4±5.9
α_D [°±SD]	88.2 ± 5.0	90.0±7.1	91.3±4.6	91.0±5.9

Table 4. The results of the Wilcoxon test (*p*-value) for comparison of medians of the sides (B_1, B_2, B_3, B_4) and angles (α_T, α_U, α_N, α_D) of fringe I and II of isochromatics

	Adults		Children	
	fringe I	**fringe II**	**fringe I**	**fringe II**
B_1 vs. B_2	0.040*	0.144	0.004*	0.331
B_1 vs. B_3	<0.001*	0.006*	0.009*	0.753
B_1 vs. B_4	<0.001*	0.030*	<0.001*	0.092
B_2 vs. B_3	<0.001*	0.162	<0.001*	0.376
B_2 vs. B_4	0.010*	0.002*	0.019*	0.440
B_3 vs. B_4	<0.001*	0.001*	<0.001*	0.219
α_T vs. α_U	0.044*	0.029*	0.458	0.219
α_T vs. α_N	<0.001*	0.001*	0.003*	0.440
α_T vs. α_D	<0.001*	0.073	0.710	0.137
α_U vs. α_N	<0.001*	0.002*	<0.001*	0.030*
α_U vs. α_D	0.057	0.925	0.607	0.475
α_N vs. α_D	0.040*	0.002*	<0.001*	0.007*

* denotes statistical significance

Figure 1:

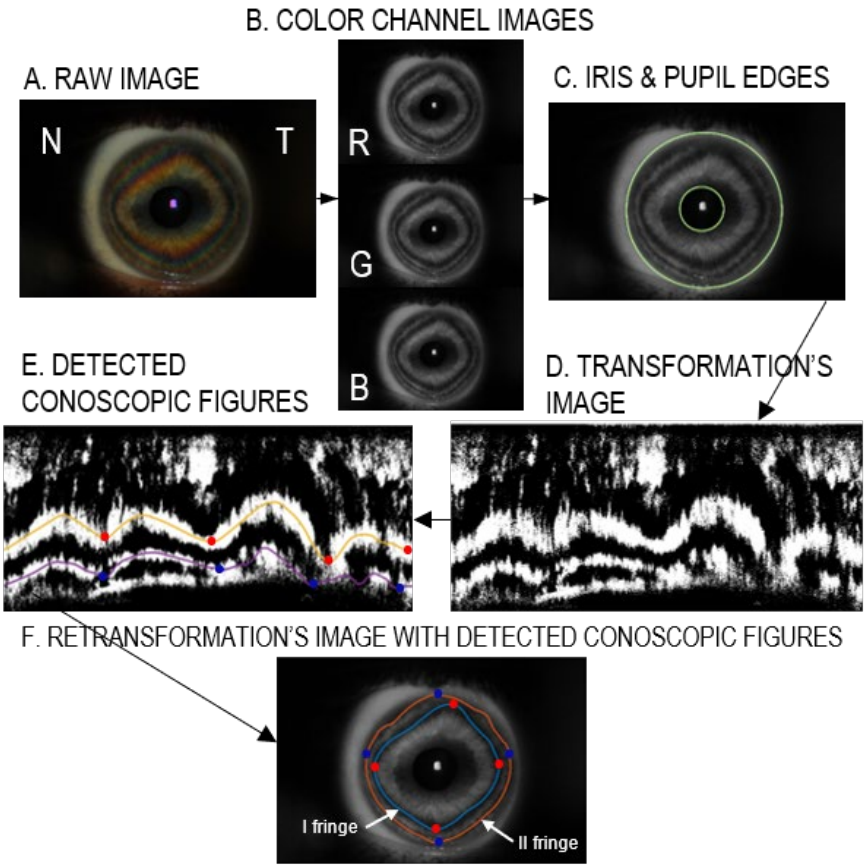

Figure 1. Block diagram of image analyzing process. Raw image (1A) is separated into color channel images (1B), the iris and pupil borders are distinguished (1C), the image is transformed into a polar system (1D), the lines responsible for isochromatics are detected as well as the inflection points (red and blue dots) (1E) after which lengths of the sides and angles are detected (1F)

Figure 2:

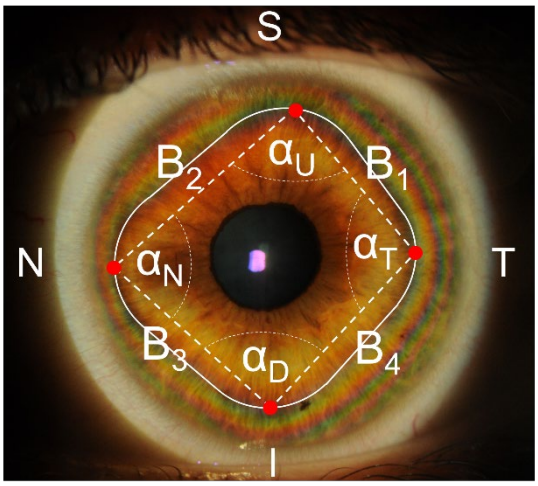

Figure 2. Shape of a quasi-rhomboid isochromatic fringe with two axes: temporal (T)-nasal (N) and superior (S)-inferior (I) , the lengths of the sides (B_1, B_2, B_3 and B_4), angles between sides of isochromatics (α_T, α_U, α_N, α_D), inflection points (red dots)

Figure 3:

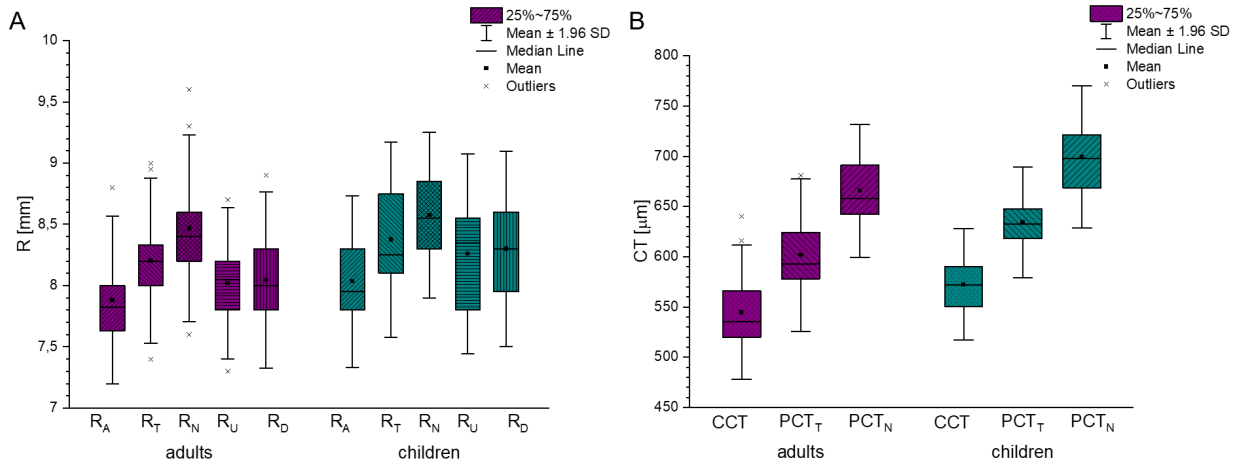

Figure 3. Boxplots of mean and median of corneal radii (R_A – axial radius, R_T – temporal radius, R_N – nasal radius, R_U – up radius, R_D- down radius) and corneal thickness (CCT – central corneal thickness, PCT_T – temporal peripheral thickness, PCT_N – nasal peripheral thickness) in groups of children and adults

Figure 4:

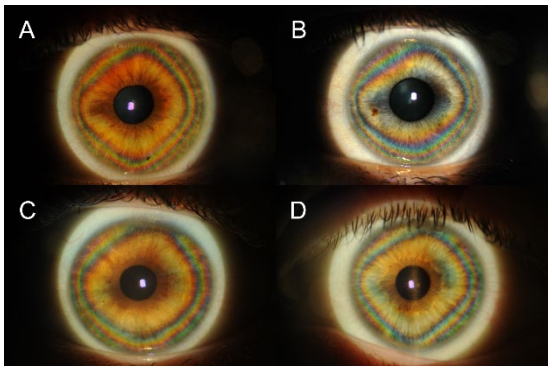

Figure 4. Exemplary images of the cornea with isochromatics from adults (A and B) and children (C and D)

Figure 5:

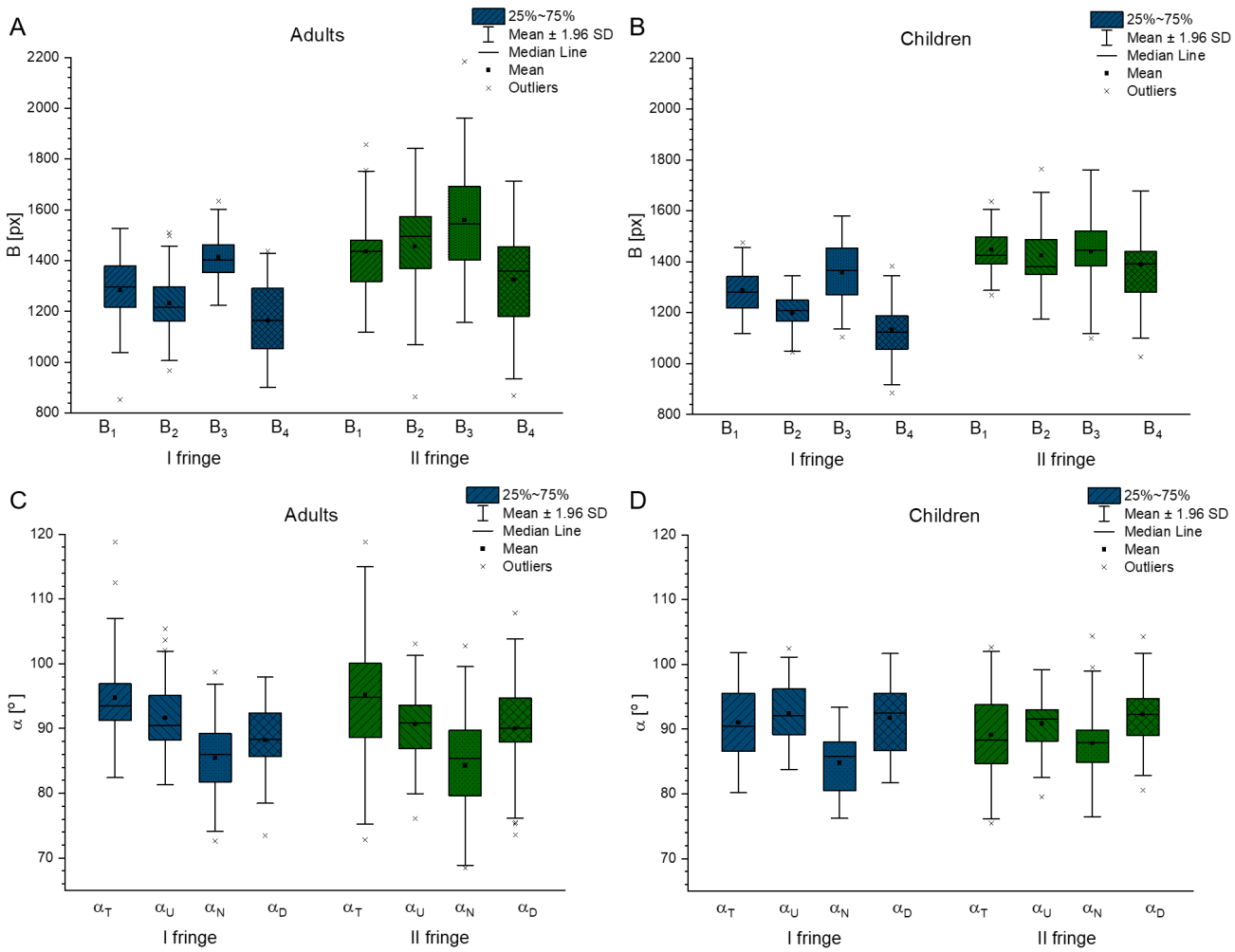

Figure 5. Boxplots of the lengths of the sides (B_1, B_2, B_3 and B_4) and angles (α_T –temporal part, α_U –upper part, α_N –nasal part, α_D – down part of cornea)

Figure 6:

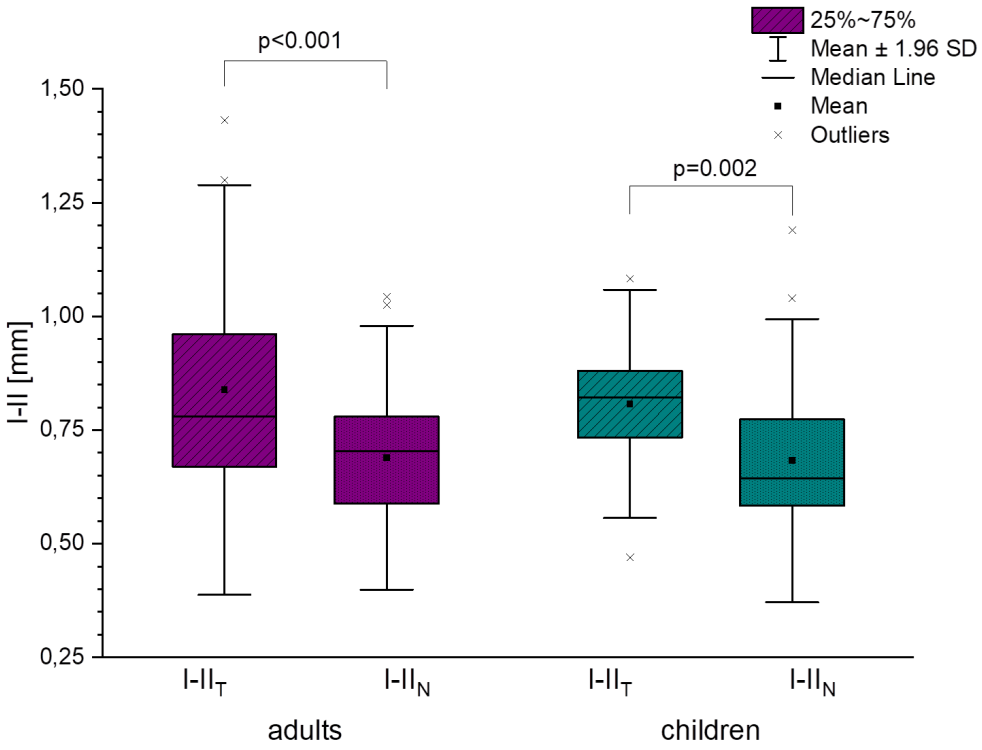

Figure 6. Boxplot of a distance between first and second fringe of isochromatics